

Phase Locking of the Boreal Summer Atmospheric Response to Dry Land Surface Anomalies in the Northern Hemisphere

HAILAN WANG

Science Systems and Applications, Inc., Lanham, Maryland

SIEGFRIED D. SCHUBERT

Science Systems and Applications, Inc., Lanham, and Global Modeling and Assimilation Office, NASA GSFC, Greenbelt, Maryland

RANDAL D. KOSTER

Global Modeling and Assimilation Office, NASA GSFC, Greenbelt, Maryland

YEHUI CHANG

Global Modeling and Assimilation Office, NASA GSFC, Greenbelt, and Morgan State University, Baltimore, Maryland

(Manuscript received 20 April 2018, in final form 15 November 2018)

ABSTRACT

Past modeling simulations, supported by observational composites, indicate that during boreal summer, dry soil moisture anomalies in very different locations within the U.S. continental interior tend to induce the same upper-tropospheric circulation pattern: a high anomaly forms over west-central North America and a low anomaly forms to the east. The present study investigates the causes of this apparent phase locking of the upper-level circulation response and extends the investigation to other land regions in the Northern Hemisphere. The phase locking over North America is found to be induced by zonal asymmetries in the local basic state originating from North American orography. Specifically, orography-induced zonal variations of air temperature, those in the lower troposphere in particular, and surface pressure play a dominant role in placing the soil moisture–forced negative Rossby wave source (dominated by upper-level divergence anomalies) over the eastern leeside of the Western Cordillera, which subsequently produces an upper-level high anomaly over west-central North America, with the downstream anomalous circulation responses phase locked by continuity. The zonal variations of the local climatological atmospheric circulation, manifested as a climatological high over central North America, help shape the spatial pattern of the upper-level circulation responses. Considering the rest of the Northern Hemisphere, the northern Middle East exhibits similar phase locking, also induced by local orography. The Middle Eastern phase locking, however, is not as pronounced as that over North America; North America is where soil moisture anomalies have the greatest impact on the upper-tropospheric circulation.

1. Introduction

Land–atmosphere coupling provides an important source of subseasonal to seasonal predictability over North America during the warm season (e.g., Koster et al. 2011). While atmospheric processes (e.g., precipitation deficits) play an obvious role in forcing land surface soil moisture anomalies, there is increasing

evidence that a regional dry soil moisture anomaly can enhance the probability of certain large-scale atmospheric circulation patterns, which may in turn reinforce the original dry land anomaly, constituting a positive land–atmosphere feedback loop. For example, Koster et al. (2014, 2016) found through modeling studies that the upper-level atmospheric circulation response to various regional dry soil moisture anomalies in the U.S. continental interior consists of a high anomaly that forms over west-central North America and a low anomaly that forms to the east, regardless of the specific

Corresponding author: Dr. Hailan Wang, hailan.wang-1@nasa.gov

DOI: 10.1175/JCLI-D-18-0240.1

© 2019 American Meteorological Society. For information regarding reuse of this content and general copyright information, consult the [AMS Copyright Policy \(www.ametsoc.org/PUBSReuseLicenses\)](https://www.ametsoc.org/PUBSReuseLicenses).

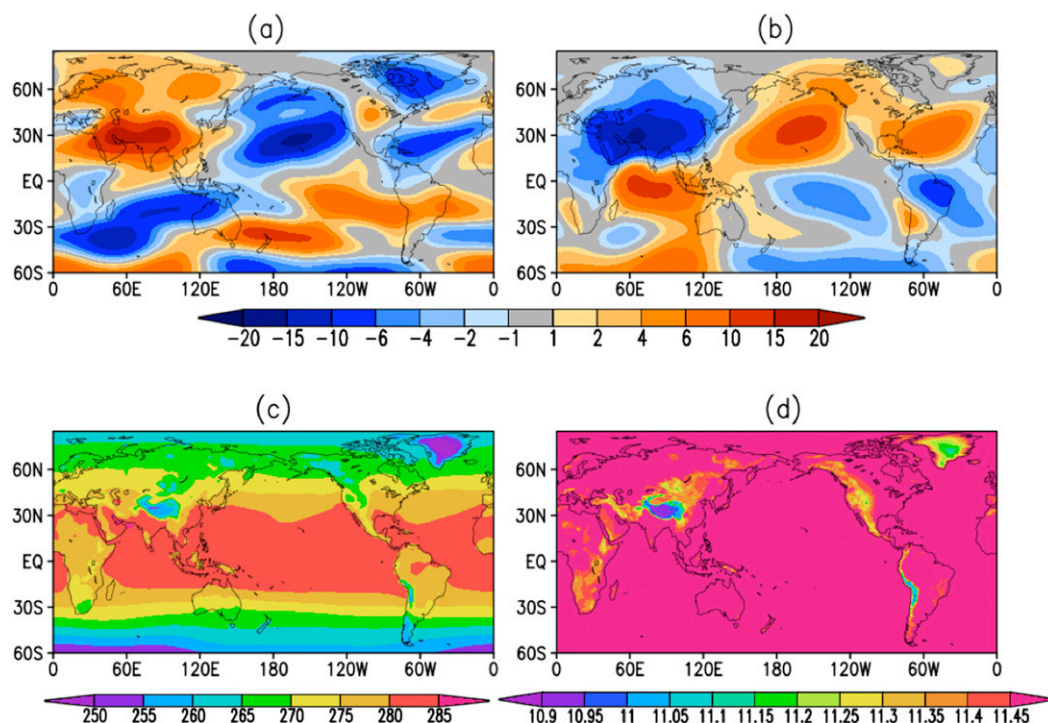


FIG. 1. (a) The JJA climatological (1992–2014) eddy streamfunction ($10^6 \text{ m}^2 \text{ s}^{-1}$) at $\sigma = 0.257$ in MERRA-2. (b) As in (a), but for eddy streamfunction ($10^6 \text{ m}^2 \text{ s}^{-1}$) at $\sigma = 0.866$. (c) As in (a), but for T (K) at $\sigma = 0.68$. (d) As in (a), but for logarithm of surface pressure (Pa).

location of the soil moisture anomaly. Such phase locking of the upper-level atmospheric circulation anomalies was found to occur both in atmospheric general circulation model (AGCM) simulations in which the land surface in various regions was artificially dried by zeroing local precipitation before it reached the land surface and in simple stationary wave model (SWM) experiments forced with idealized diabatic heating anomalies that mimic those produced by the local dry land surface anomalies in the AGCM simulations. Furthermore, both the AGCM-based and SWM-based patterns generally agree with observational composites based on continental-scale soil moisture dryness (Koster et al. 2016)—that is, the simulated phase-locked patterns are supported by the observational data.

The phase locking of the upper-level circulation anomalies, as seen in the models, is intriguing, and its cause is unclear. It is presumably associated with zonal asymmetries in the three-dimensional (3D) summertime climatological basic state, which consists of zonal variations of zonal wind, meridional wind, air temperature, and surface pressure. In the upper troposphere, the zonal variations of the Northern Hemisphere summertime atmospheric circulation—namely, stationary waves—include the Asian monsoonal anticyclones centered over the Tibetan Plateau and the Iranian Plateau and the oceanic

subtropical troughs in the North Pacific and North Atlantic (Fig. 1a); in the lower troposphere, they include the Asian monsoonal low, the North Pacific subtropical high, and the North Atlantic subtropical high (Fig. 1b). These circulation features are largely baroclinic and are maintained by global diabatic heating (e.g., Ting 1994; Rodwell and Hoskins 2001). Over North America, the dominant summertime circulation feature is a barotropic high that resides over the western two-thirds of North America (Fig. 1a) and peaks in the midtroposphere (not shown). The low-level circulation over the central United States is dominated by the Great Plains low-level jet (Fig. 1b) (LLJ; e.g., Bonner 1968; Helfand and Schubert 1995). Past stationary wave modeling studies have shown that these circulation features over North America are maintained by the nonlinear interaction between orography and atmospheric flow forced by diabatic heating (e.g., Ting 1994; Ting et al. 2001; Ting and Wang 2006). For example, the time-mean Great Plains LLJ forms as the trade winds along the southern flank of the North Atlantic subtropical high turn northward upon encountering the Sierra Madre Oriental and obtains anticyclonic shear vorticity (Ting and Wang 2006). The zonal variations of air temperature and surface pressure are strongly affected by orography. At a given σ level in the atmosphere, where σ is defined as the ratio of the pressure of

the level to surface pressure, regions with mountains tend to be colder than those without mountains (Fig. 1c). We note that the opposite is true for the comparison of temperature in pressure coordinates, where at a given pressure level regions at higher elevations (e.g., with mountains) tend to be warmer than those at lower elevations (not shown). Surface pressure has the direct imprint of orography (Fig. 1d): the higher the surface elevation, the lower the surface pressure.

Building on the work of Koster et al. (2016), this study focuses on the physical mechanisms by which zonal asymmetries in the climatological basic state appear to phase lock the upper-level atmospheric circulation anomalies forced by dry land conditions over the U.S. continental interior. The problem is addressed with both an SWM analysis of the processes maintaining the relevant components of the 3D basic state and idealized AGCM experiments that specifically isolate the impacts of North American orography and land–sea contrast on the phase locking. The investigation is then extended to other regions of the Northern Hemisphere.

2. Models and experiments

a. NASA GEOS AGCM and experiments

The NASA GEOS AGCM is used here to isolate the separate effects of orography and land–sea contrasts in maintaining the summertime climate that induces the phase locking. The GEOS AGCM (Rienecker et al. 2008; Molod et al. 2012) is a state-of-the-art atmospheric modeling system maintained by the Global Modeling and Assimilation Office (GMAO) at NASA's Goddard Space Flight Center. The GEOS AGCM used in this study is the version underlying the recent Modern-Era Retrospective Analysis for Research and Applications, version 2 (MERRA-2) (Gelaro et al. 2017). This version (with internal designation Ganymed_4_0) employs the finite-volume dynamics of Lin (2004). Its various physics packages (Bacmeister et al. 2006) include a modified form of the relaxed Arakawa–Schubert convection scheme (Moorthi and Suarez 1992) with stochastic Tokioka limits on plume entrainment (Tokioka et al. 1988), prognostic cloud microphysics (Bacmeister et al. 2006), and the catchment land surface model (Koster et al. 2000).

North American orography and land–sea contrast are presumably the main drivers for the zonal asymmetries in the summertime climatological circulation over North America. To investigate their separate roles in determining the summertime climatology, we performed two GEOS AGCM runs, one with the default representation of North American orography (the “M” run, where M stands for mountains) and one in which the orography is

removed; that is, the North American continent is made artificially flat (the “noNA” run, where NA stands for North American mountains). Both runs were integrated from 1989 to 2014, forced with observed sea surface temperature (SST) and sea ice fraction based on the 1° resolution weekly product of Reynolds et al. (2002), as well as time-varying greenhouse gases (see Schubert et al. 2014 for more details). The first three years (1989–91) of both runs were discarded as spinup, so the summertime climatology examined here is the mean of June–August (JJA) averaged over the period 1992–2014. Our analysis of these AGCM runs is focused solely on their boreal summer climatologies, which should be robustly determined from the 23-yr simulation period (1992–2014). We note that the linear trends of the basic-state variables over the period 1992–2014 are modest: their impacts on the mean basic state and the subsequent SWM solutions (forced by imposed regional idealized heating anomalies) are small overall. The influence of North American orography on the summertime climate is assessed by comparing the M and noNA runs, with a focus on the character of the climatological basic-state variables. The effect of the land–sea contrast on the summertime climatology is studied by examining the zonal asymmetry of the 3D climatological basic state in the noNA run. As will be discussed in section 3b, the zonal asymmetries of climatological atmospheric circulation over North America in the noNA simulation arise primarily from diabatic heating anomalies caused by land–sea contrasts associated with the North American continent.

Our investigation also identifies the northern Middle East as another region in the Northern Hemisphere that exhibits the phase-locking behavior (see section 3c). To investigate the role of local orography in inducing the phase locking over the northern Middle East, we performed a third AGCM experiment in which the Iranian Plateau is removed; that is, the local topography there is flattened (the “noIP” run, where IP stands for the Iranian Plateau). The effect of the Iranian Plateau is then determined by comparing the noIP run with the M run.

While AGCMs have been an important tool for studying the role of orography on the nature of Earth's climate (e.g., Nigam et al. 1986; Broccoli and Manabe 1992; Ting and Wang 2006), a few potential caveats are worth noting. First, since SST and sea ice are prescribed, the runs do not realistically account for any impact (and possible subsequent feedback) of orography on the oceanic boundary conditions (e.g., Kitoh 2002). Second, the vegetation and soil types prescribed in the noNA and noIP runs match those of the M run, despite the fact that orography has an obvious impact on the character of these boundary conditions. We assume here that accounting accurately for these issues would have

at most a secondary impact on the large-scale atmospheric circulation (Yasunari et al. 2006), particularly in the upper troposphere, which is the focus of this study; that is, ignoring ocean feedbacks and orography-dependent boundary conditions should not impact our main conclusions.

b. Experiments with a nonlinear stationary wave model

A nonlinear stationary wave model (Ting and Yu 1998) is used here for several purposes: (i) to identify regional phase locking that occurs in the Northern Hemisphere, (ii) to determine those aspects of the regional climatological basic state that control the phase locking, and (iii) to diagnose the maintenance of summertime climatological stationary waves induced by orography as simulated by the GEOS AGCM (section 2a). The SWM, which is based on the 3D primitive equations in σ coordinates, is time dependent and nonlinear. The model has rhomboidal wavenumber-30 truncation in the horizontal and 14 unevenly spaced σ levels in the vertical. The inputs for the SWM include a specified basic state and fixed stationary wave forcings. The basic state is derived from fields from a reanalysis or an AGCM simulation, consisting of 3D zonal wind U , meridional wind V , air temperature T , and a logarithm of 2D surface pressure P_s , which can be zonally averaged or zonally varying. The stationary wave forcings consist of orography, diabatic heating, and transient flux convergences. The model has been shown to be a valuable tool for diagnosing the maintenance of the climatological atmospheric circulation as well as circulation anomalies on various time scales (e.g., Ting and Yu 1998; Schubert et al. 2011). See Ting and Yu (1998) for a detailed description of the model. Tables 1–3 list the stationary wave experiments performed in this study.

The SWM is used to identify regional phase locking in the Northern Hemisphere. Koster et al. (2016) found phase-locking behavior over North America both in AGCM simulations forced with regional dry land surface anomalies and in simpler SWM experiments forced with idealized heating anomalies that mimic those induced by a regionally dry land surface. Because of its simplicity and ease of use, the SWM is chosen over the AGCM in the present study to search for regional phase locking outside of North America. Following Koster et al. (2016), the areal extent of the imposed heating anomaly in the SWM is given horizontal half-widths of 5° longitude and 5° latitude, as indicated using region 4 in Fig. 2; the Fig. 2 inset illustrates the vertical profile of the imposed heating anomaly. The horizontal and vertical distributions of the imposed idealized heating anomaly in Fig. 2 are consistent with those produced by the locally dried land surfaces in the GEOS AGCM simulations of Koster et al. (2016). For

TABLE 1. Stationary wave model runs performed to identify phase locking in the Northern Hemisphere.

Experiment	Basic state	Data used	
		to derive basic state	Stationary wave forcing
A0	3D	MERRA-2	Idealized heating anomalies placed every 7° in longitude (0.5° – 357.5° E) and every 7° in latitude (5.5° – 68.5° N) across the Northern Hemisphere

the identification of regional phase locking, an extensive series of SWM experiments is performed (A0 in Table 1) that consists of independent runs forced with regional idealized heating anomalies placed every 7° in longitude (0.5° – 357.5° E) and every 7° in latitude (5.5° – 68.5° N) across the Northern Hemisphere (520 runs in total), each run using the zonally varying summertime climatological basic state from MERRA-2. (The regions covered by 13 of these SWM simulations are indicated in Fig. 2.) The SWM results are then examined to identify regional phase locking. We note that the SWM results presented here are basically insensitive to the specific reanalysis used to construct the climatological basic state; the results from test runs with basic states constructed using other reanalyses (e.g., MERRA, NCEP–NCAR reanalysis) agree very well with those based on MERRA-2 (not shown).

As will be shown, the analysis identifies two regions of phase locking, namely, North America and the northern Middle East. For both regions, a number of additional SWM experiments (see Tables 2, 3) are performed and analyzed to determine the aspects of the climatological basic state that induce the phase locking. Each of these SWM experiments consists of several runs, with each run imposing an idealized diabatic heating anomaly over one of the regions defined in Fig. 2, using the vertical heating profile indicated in the Fig. 2 inset. Specifically, each of the SWM experiments for the phase locking over North America consists of seven runs, forced with an idealized heating anomaly imposed at regions 1–7, respectively. Likewise, each of the SWM experiments for the northern Middle East consists of six runs, forced with an idealized heating anomaly imposed at regions i1–i6, respectively. These SWM experiments differ only in the summertime climatological basic state they use (e.g., zonally varying or zonally averaged globally, or a combination of the two over separate regions, taken from either the MERRA-2 or the GEOS AGCM simulations). The basic states and stationary wave forcings used are described in detail in Tables 2 and 3, and they will also be described in section 3, where the results are presented.

TABLE 2. List of stationary wave model experiments performed to investigate the phase locking over North America. Note that A1 is a subset of the A0 runs (Table 1).

Expt	Basic state	Data used to derive basic state	Stationary wave forcing
A1	3D	MERRA-2	Idealized heating anomalies imposed at regions 1–7
A2	Zonal mean	MERRA-2	Idealized heating anomalies imposed at regions 1–7
A3	3D over 120°–60°W, zonal mean elsewhere	MERRA-2	Idealized heating anomalies imposed at regions 1–7
A4	Zonal mean over 120°–60°W, 3D elsewhere	MERRA-2	Idealized heating anomalies imposed at regions 1–7
A5	3D <i>T</i> and <i>Ps</i> , zonal mean <i>U</i> and <i>V</i>	MERRA-2	Idealized heating anomalies imposed at regions 1–7
A6	Zonal mean <i>T</i> and <i>Ps</i> , 3D <i>U</i> and <i>V</i>	MERRA-2	Idealized heating anomalies imposed at regions 1–7
B1	3D	noNA simulation	North American orography (NA_oro)graphy)
B2	3D	noNA simulation	Diabatic heating difference between M and noNA simulations (M minus noNA) (NA_heating)
B3	3D	noNA simulation	NA_oro)graphy plus NA_heating
C1	3D	M simulation	Idealized heating anomalies imposed at regions 1–7
C2	3D	noNA simulation	Idealized heating anomalies imposed at regions 1–7
C3	Zonal mean	noNA simulation	Idealized heating anomalies imposed at regions 1–7

Finally, to better understand the effect of orography on the distribution of regional climatological stationary waves, we use the SWM to diagnose the maintenance of the climatological stationary wave differences seen between our GEOS AGCM simulations with and without orography. Here the SWM experiments use the 3D climatological basic state from the AGCM simulation without orography (e.g., the noNA run) and are forced with the diagnosed stationary wave forcing differences between the AGCM simulations with and without orography (e.g., the M vs noNA simulations); these forcing differences include orography itself and the diabatic heating changes induced by the orography. We note that the diabatic heating is taken directly from the AGCM output: we do not add the contributions from transient heat flux convergences to it. In fact, the changes in transient flux convergences induced by the orography are not considered here given their overall small contribution to climatological stationary waves in the summer hemisphere

(e.g., Ting and Wang 2006). Specifically, SWM experiments B1–B3 in Table 2 are used to diagnose the climatological stationary waves maintained by North American orography, whereas experiments E1–E3 in Table 3 diagnose the climatological stationary waves forced by the Iranian Plateau.

In the aforementioned SWM runs, with the specified basic state and fixed stationary wave forcing(s), the SWM reaches a steady state after being integrated for about 20 days. The stationary wave model responses are then obtained by averaging the model solutions over days 31–50.

3. Results

a. Basic-state controls on phase locking over North America

To isolate those aspects of the 3D climatological basic state that control phase locking over North America, we

TABLE 3. List of stationary wave model experiments performed to investigate the phase locking over the northern Middle East. Note that D1 is a subset of the A0 runs (Table 1).

Expt	Basic state	Data used to derive basic state	Stationary wave forcing
D1	3D	MERRA-2	Idealized heating anomalies imposed at regions i1–i6
D2	3D over 0°–65°E, zonal mean elsewhere	MERRA-2	Idealized heating anomalies imposed at regions i1–i6
D3	Zonal mean over 0°–65°E, 3D elsewhere	MERRA-2	Idealized heating anomalies imposed at regions i1–i6
D4	3D <i>T</i> and <i>Ps</i> , zonal mean <i>U</i> and <i>V</i>	MERRA-2	Idealized heating anomalies imposed at regions i1–i6
E1	3D	noIP simulation	Iranian Plateau orography (IP_oro)graphy)
E2	3D	noIP simulation	Diabatic heating difference between M and noIP simulations (M minus noIP) (IP_heating)
E3	3D	noIP simulation	IP_oro)graphy plus IP_heating
F1	3D	M simulation	Idealized heating anomalies imposed at regions i1–i6
F2	3D	noIP simulation	Idealized heating anomalies imposed at regions i1–i6

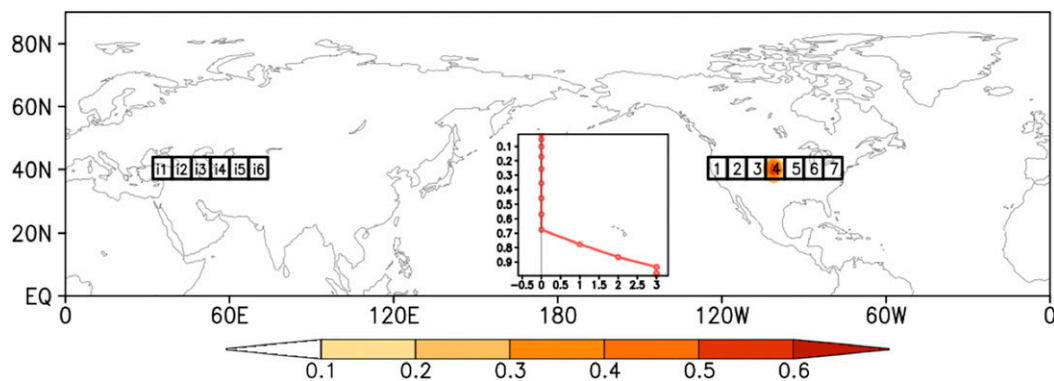


FIG. 2. Regions of imposed diabatic heating anomaly considered in the SWM experiments (labeled 1–7 over North America, and i1–i6 over the northern Middle East), and spatial distribution of the imposed idealized heating anomaly (shaded; K day^{-1}) near the ground surface (model sigma level $\sigma = 0.9966$) for region 4. (inset) Vertical profile of idealized diabatic heating anomaly (K day^{-1}) imposed in the SWM atmosphere over a selected geographical area.

performed four SWM experiments (A1–A4 in Table 2) that differ from each other only in the underlying climatological basic state employed. All of the basic states used here were derived from the recent NASA MERRA-2 reanalysis (Gelaro et al. 2017). The four experiments use respectively 1) a 3D zonally varying basic state (i.e., one that captures the full complexity of the climatological atmospheric circulation), 2) a zonal mean basic state, 3) a 3D zonally varying basic state over North America (120° – 60°W) and a zonal mean basic state elsewhere, and 4) a zonal mean basic state over North America (120° – 60°W) and a 3D zonally varying basic state elsewhere. While the juxtaposition of a regional zonal mean basic state and a 3D zonally varying basic state in experiments 3 and 4 is rather artificial, it has been shown to be an effective approach for isolating and assessing the effect of a 3D zonally varying basic state over a specific region (e.g., Ting and Wang 2006).

The basic character of the phase locking is illustrated by the SWM experiment A1, which uses the full 3D zonally varying JJA mean basic state (Fig. 3). It is clear from Figs. 3a–g that although the heating anomalies imposed at regions 2–6 are at very different longitudes in the United States, the basic spatial pattern of their forced upper-level atmospheric circulation response is mostly the same: a high anomaly forms over west-central North America and a low anomaly forms over the east. The vertical distribution of the responses (averaged over 35° – 50°N) is also similar between these SWM runs: the high anomaly over west-central North America peaks in the upper troposphere and extends down to the lower troposphere, while the downstream low anomaly mainly occurs in the upper troposphere (Figs. 3h–n).

This similarity constitutes the phase locking examined in this paper. It is expressed more succinctly in Fig. 4b, which shows, as a function of longitude, the upper-level

atmospheric circulation responses averaged between 35° and 50°N for each of the seven SWM runs that use the 3D zonally varying JJA mean basic state. The spatial pattern of the phase-locked circulation anomaly is exemplified in Fig. 4a, using the upper-level circulation response to the heating anomaly imposed at region 4. The y axis in Fig. 4b is keyed to the run number; that is, the shading at a given y value is based on the responses produced in the corresponding SWM run. To see, for example, the average streamfunction response as a function of longitude when a heating anomaly is located over region 3 in Fig. 2, one simply needs to read the values displayed in Fig. 4b for $y = 3$. Note that if the circulation response to a heating anomaly moved in tandem with the heating anomaly's location, then the shading contours in Fig. 4b would appear as diagonal lines. Such diagonality, however, is essentially absent here. The salient feature of Fig. 4b is the “blockiness” of the pattern—the fact that the longitudes of the maxima and minima are roughly the same in the different runs, particularly for the runs with the heating anomalies imposed over regions 2–6. Blockiness in this kind of plot is indeed an intrinsic signature of the phase-locking behavior being examined here.

Again, four separate seven-run SWM experiments (A1–A4) were performed, each making a different assumption about the character of the underlying climatological basic state (section 2b). Figures 4c and 4d, Figs. 4e and 4f, and Figs. 4g and 4h repeat Figs. 4a and 4b (A1) for the experiments A2, A3, and A4, respectively. Phase locking is clearly seen only when the 3D zonally varying basic state over North America is used (Figs. 4a,b,e,f); it disappears when the zonal mean basic state is prescribed over North America (Figs. 4c,d,g,h). The zonal variations of the local basic state are thus critical to the

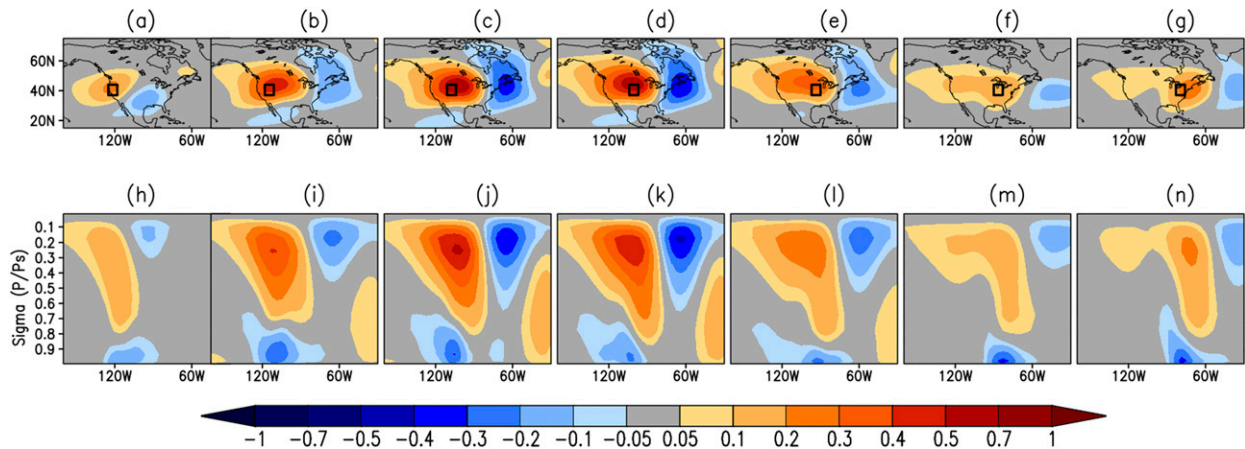


FIG. 3. (a)–(g) The spatial distribution of the eddy streamfunction response ($10^6 \text{ m}^2 \text{ s}^{-1}$) at $\sigma = 0.257$ to the idealized diabatic heating anomaly imposed at regions 1–7 (the seven regions are indicated using black boxes; see Fig. 2 for their definitions), as produced by the SWM with a 3D zonally varying JJA mean basic state from MERRA-2 for the period 1992–2014. (h)–(n) Vertical profile of the eddy streamfunction response averaged between 35° and 50°N .

phase locking. They also greatly strengthen the upper-level circulation responses and shape their spatial pattern (e.g., cf. Fig. 4a with Fig. 4c).

The zonal variations of the basic state over North America consist of the climatological high in the mid- and upper troposphere (Fig. 1a), the Great Plains LLJ in the lower troposphere (Fig. 1b), and distinct geographical variations of T (Fig. 1c) and P_s (Fig. 1d) that are closely tied to North American topography. We are interested here in isolating the contribution of the zonal variations of atmospheric circulation (U , V) to the phase locking from that of the zonal variations of T and P_s . Two additional SWM experiments, A5 and A6, were therefore performed: A5 uses a basic state with zonal mean U and V and zonally varying T and P_s (Figs. 5a,b), whereas A6 uses a basic state with zonally varying U and V and zonal mean T and P_s (Figs. 5c,d). A comparison of the results in Fig. 5 with those in Figs. 4a and 4b clearly shows that zonal variations of T and P_s play a key role in maintaining the phase locking as well as in accounting for much of the magnitude of the upper-level circulation response. Two additional SWM experiments (not shown) were performed that are identical to A5 but in their basic state use respectively 1) zonally varying T near surface (σ from 1 to 0.98) and zonal mean T above that, and 2) zonally varying T in the lower troposphere (σ from 1 to 0.78) and zonal mean T above that. The comparison of those results with A5 shows that it is primarily the zonal variations of T in the lower troposphere, those near surface in particular, and P_s that produce the phase locking. The spatial pattern of the phase-locked circulation response (Fig. 5a), particularly that of the low-anomaly response along the eastern United States, however, differs from that of the response when the 3D basic state is used (Fig. 4a). It

instead resembles the response with the zonal mean basic state (Fig. 4c), in which the downstream low anomaly has a southwest–northeast tilt and the high anomaly over west-central North America also does not extend to 80°W as seen in Fig. 4a. By comparison, while the upper-level circulation anomalies induced by the zonal variations of U and V are weak and do not contribute strongly to phase locking, they nevertheless contribute to shaping the spatial pattern of upper-level circulation responses and bring it closer to the observed (Figs. 5c,d). Thus, the phase locking of the upper-level circulation response in Figs. 4a and 4b is maintained by zonal asymmetries of all the basic-state variables, with the zonal asymmetries of T and P_s playing a key role in maintaining the phase locking and those of atmospheric circulation shaping the spatial pattern of the circulation response.

In an attempt to understand the dynamical mechanisms associated with the phase locking, we computed the Rossby wave source (RWS) (Sardeshmukh and Hoskins 1988) for the upper-level circulation response in the SWM:

$$\begin{aligned} \text{RWS} = & -\mathbf{V}'_x \cdot \nabla(\bar{\zeta} + f) - \bar{\mathbf{V}}_x \cdot \nabla\zeta' - (\bar{\zeta} + f)\nabla \cdot \mathbf{V}'_x \\ & - \zeta'\nabla \cdot \bar{\mathbf{V}}_x, \end{aligned} \quad (1)$$

where \mathbf{V}_x is the divergent wind vector, ζ is the relative vorticity, f is the Coriolis parameter, and the overbar and prime indicate the climatological basic state and the SWM response to an imposed idealized heating anomaly, respectively. A caveat in applying this analysis here is that the RWS anomalies essentially arise from the forced atmospheric circulation anomalies, so the RWS diagnosis is unlikely to help establish cause-and-effect relationships.

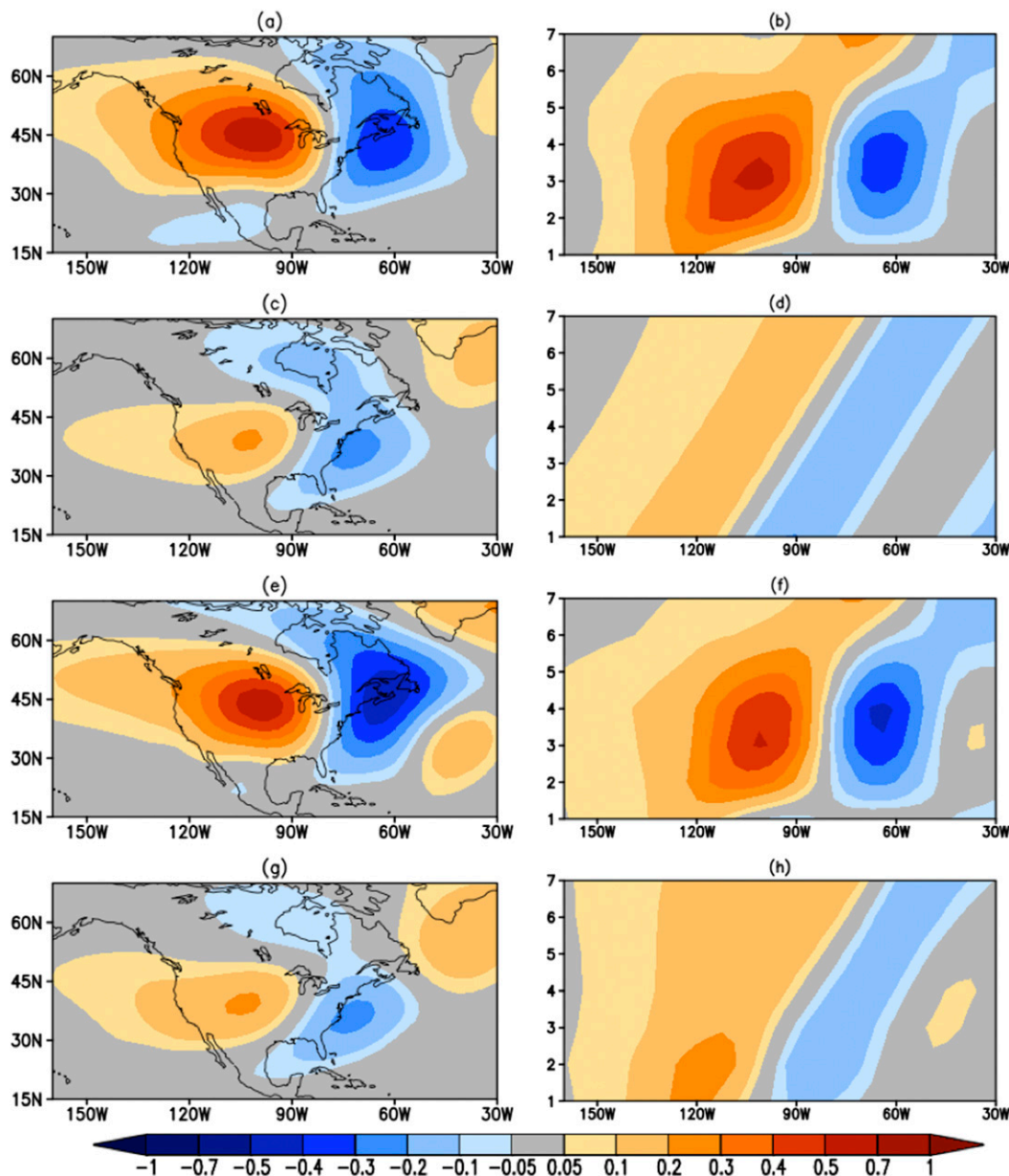


FIG. 4. (a) The spatial distribution of the eddy streamfunction response at $\sigma = 0.257$ to the idealized diabatic heating anomaly imposed at region 4, to illustrate the phase-locked circulation pattern. (b) The eddy streamfunction response at $\sigma = 0.257$ averaged between 35° and 50°N for regions 1–7 (y axis: region number); the shading for $y = 4$, for example, shows the results for the experiment with the heating anomaly imposed over region 4. Note that without the phase locking, the contours would appear as diagonal lines. (c),(d) As in (a) and (b), respectively, but for the SWM runs that use the zonal mean basic state from MERRA-2. (e),(f) As in (a) and (b), respectively, but for the SWM runs that use the 3D zonally varying basic state over the North American domain (120° – 60°W) and a zonal mean basic state elsewhere. (g),(h) As in (a) and (b), respectively, but for the SWM runs that use the zonal mean basic state over the North American domain (120° and 60°W) and a 3D zonally varying basic state elsewhere. Units: $10^6 \text{ m}^2 \text{ s}^{-1}$.

Nevertheless, as shown below, the RWS diagnosis can help us determine the dominant processes and better understand the dynamics of the SWM solutions.

In the context of the SWM experiments, an imposed near-surface local heating anomaly excites anomalous

ascendance, which induces convergence at the surface and divergence in the middle and upper troposphere. The strongest divergence response occurs in the lower midtroposphere, but the response there moves in tandem with the imposed heating anomalies and is not phase

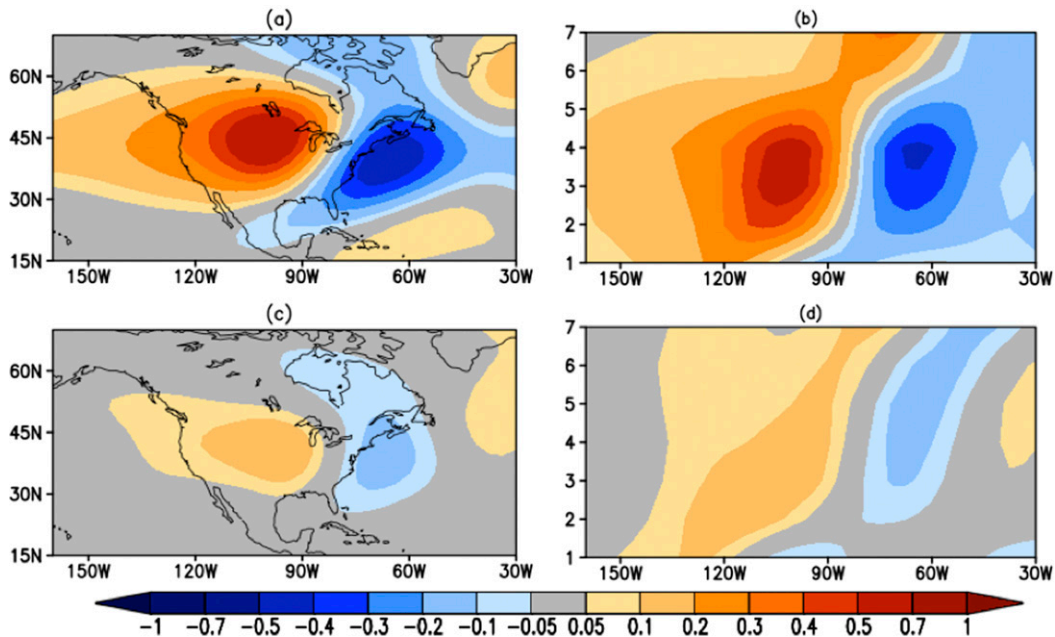


FIG. 5. (a),(b) As in Figs. 4a and 4b, respectively, but for the SWM runs that use a MERRA-2 basic state derived using zonal mean U and V and zonally varying T and Ps . (c),(d) As in (a) and (b), respectively, but for a MERRA-2 basic state derived using zonally varying U and V and zonal mean T and Ps . Units: $10^6 \text{ m}^2 \text{ s}^{-1}$.

locked. As shown below, the divergence response in the upper troposphere, while considerably weaker, is what is relevant to the upper-level phase locking. Specifically, in the upper troposphere, the divergence response interacts with the mean basic state to produce the RWS that drives the upper-level atmospheric circulation response. Figure 6 shows that the imposed heating anomaly over region 4 leads to a strong negative vorticity source over the U.S. Great Plains in the upper troposphere, with weaker positive vorticity sources to the west and east. These vorticity sources subsequently excite an upper-level high anomaly over west-central North America and a low anomaly to the east. Not surprisingly, the upper-level RWS (Fig. 6b) displays a phase locking similar to the upper-level circulation response (Fig. 4b). A decomposition of the RWS into individual terms shows the predominant role of the stretching of the mean absolute vorticity by the forced divergence response $[-(\bar{\zeta} + f)\nabla \cdot \mathbf{V}'_x]$, the spatial distribution of which is determined by the upper-level divergence response (Fig. 6c), which displays a phase locking as well (Fig. 6d).

We attempted to provide further insight into the mechanisms by which the zonal asymmetries of T and Ps lead to the phase locking. We first examined how the individual terms in the SWM (e.g., those associated with the tendencies of upper-level vorticity and eddy streamfunction) evolve to a steady state. These additional tests, however, turned out to be of limited value.

The basic-state variables and perturbation variables in the SWM equations are too strongly intertwined to allow the isolation of clear cause-and-effect relationships. We then turned to a simple thermodynamic framework for potential temperature θ . In the framework, diabatic heating is balanced by the time tendency of θ , the horizontal transports of θ by zonal and meridional winds, and the vertical transports by vertical motion. Potential temperature is chosen here because it combines the information of T and Ps . It is warmer over regions of higher elevations than over those of lower elevations in both σ and pressure coordinates: over mountains, while the temperature is colder, the pressure is also lower; the effect of the decrease in pressure on θ overwhelms that of the decrease in temperature, resulting in warmer θ there. Over North America, θ is considerably warmer over the high-elevation Western Cordillera than over the rest of the continent to the east, which leads to considerable horizontal gradients over much of the North American continental interior. Now consider a case in which a heating anomaly is imposed in the continental interior and the zonal mean of the climatological θ is used in the basic state: the heating anomaly is largely balanced by the changes in vertical motion, because the contribution from the horizontal transports of the climatological θ is small by design. In a parallel case in which the 3D climatological θ is used in the basic state, however, the zonal asymmetry of the climatological

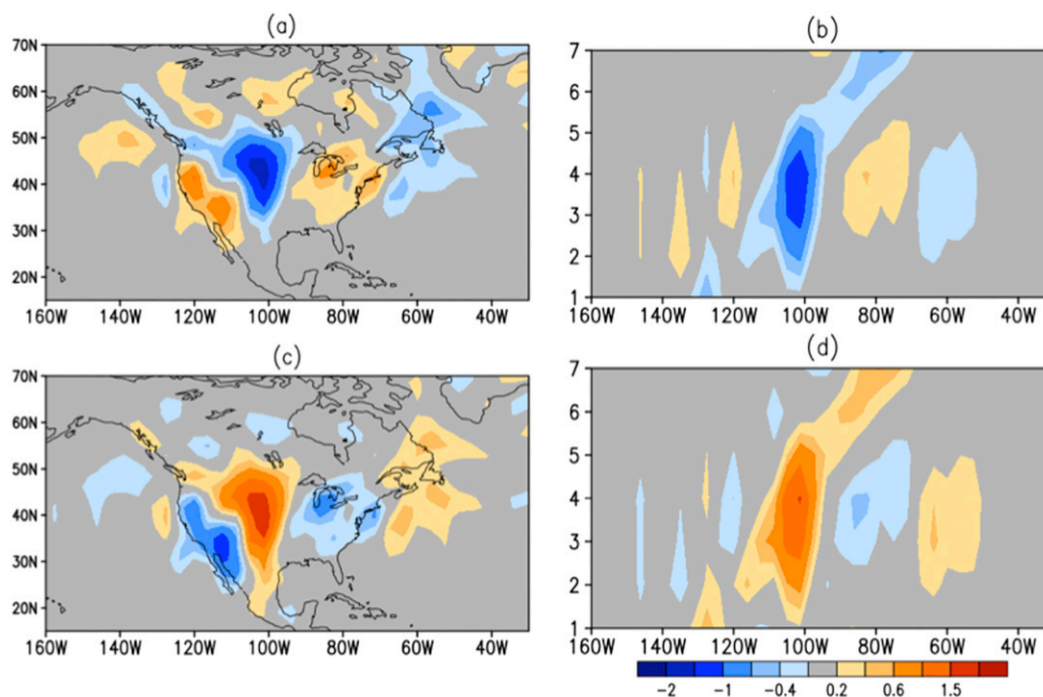


FIG. 6. (a) The RWS (10^{-11} s^{-2}) for the SWM response at $\sigma = 0.257$ to the idealized diabatic heating anomaly imposed at region 4 with the 3D climatological JJA basic state from MERRA-2. (b) The RWS at $\sigma = 0.257$ averaged between 35° and 50°N for SWM responses to idealized diabatic heating anomalies imposed at regions 1–7. (c),(d) As in (a) and (b), respectively, but for the SWM divergence responses (10^{-7} s^{-1}) at $\sigma = 0.257$.

θ would come into play: the low-level heating-induced anomalous convergent atmospheric flow would bring in warm θ air from western North America, which would subsequently enhance the anomalies in low-level convergence and ascendance; the zonal asymmetry of the climatological θ presumably also helps anchor the upper-level atmospheric responses to the central North America, where it has the greatest horizontal gradients. While the aforementioned arguments are mostly qualitative, they are supported by the SWM results. Compared to the SWM results in which the zonal mean basic state is used, the SWM results that use the 3D MERRA-2 basic state show notably stronger low-level divergence responses as well as stronger atmospheric circulation responses in both the lower and upper troposphere (not shown). Furthermore, the upper-level temperature response displays a phase-locked spatial pattern, with a warm anomaly over western-central North America and a cold anomaly over eastern North America (not shown). The phase-locked anomalous temperature responses are presumably connected with the phase-locked wind responses (e.g., Fig. 4a) via geostrophic adjustment.

Collectively, the aforementioned stationary wave modeling diagnosis and the RWS analysis point to the importance of North American topography (e.g., via its impacts on the zonal asymmetries of climatological T

in the lower troposphere and Ps) in phase locking the upper-level divergence response, and hence the RWS and upper-level circulation response. The separate roles of North American orography and land–sea contrast are investigated in the next subsection using GCM simulations.

b. Maintenance of the local base state: Relative roles of North American orography and land–sea contrast

This subsection examines the M and noNA AGCM simulations along with supplemental SWM experiments (B1–B3, C1–C3) to assess the relative roles of North American orography and land–sea contrast in contributing to the 3D basic state that induces phase locking over North America. As discussed in section 2a, the M simulation includes the default North American topography, whereas the noNA simulation is run without it—it runs instead with a flattened continental interior. The effect of orography on the distribution of local T and Ps is fairly straightforward (Figs. 1c,d) and is well captured by the GEOS AGCM, at least to the first order (not shown). Much of the discussion in this subsection thus focuses on the effect of orography on climatological stationary waves (U , V). While not key to the phase locking itself, U and V have been shown to be important

in maintaining the spatial pattern of the phase-locked circulation anomalies (Figs. 5c,d). As such, by including U and V we obtain a more complete picture of the effect of North American orography on all the basic variables that constitute the climatological base state.

The GEOS AGCM does a credible job of reproducing relevant features in the observations, as represented by MERRA-2; a comparison of Figs. 7a and 1a shows that the M simulation reproduces reasonably well the climatological stationary waves produced in the reanalysis, and the T and P_s fields from the M simulation (not shown) are similarly in agreement with the corresponding MERRA-2 fields. The comparison between the M (Fig. 7a) and noNA simulations (Fig. 7b) shows that North American orography plays a key role in shaping the local atmospheric circulation. In particular, the North American high is clearly present in the M run (Fig. 7a) but is absent in the noNA run (Fig. 7b). North American orography is also essential for shaping and strengthening the North Atlantic jet stream and storm tracks (not shown) (Brayshaw et al. 2009), which would otherwise be rather weak at their observed locations.

Like other high-elevation mountains, the North American orography can directly affect the climatological atmospheric circulation by obstructing atmospheric flow that impinges upon it, and it can indirectly affect the climatological circulation by modifying the spatial distribution of climatological diabatic heating and transient flux convergence (e.g., Ting and Wang 2006). To better understand how these factors influence the generation of the climatological high over the continent, we performed three supplemental SWM experiments (B1–B3) that use the 3D climatological basic state from the noNA AGCM simulation but have imposed on them stationary wave forcing features specific to the M simulation. Specifically, the experiments B1, B2, and B3 are respectively forced with (i) North American orography, (ii) the summertime climatological diabatic heating difference between the M and noNA runs (i.e., the modification of diabatic heating resulting from North American orography), and (iii) these two stationary wave forcings combined. The diabatic heating differences between the M and noNA runs (Fig. 7f) consist of a moderate increase over the U.S. Great Plains, a strong increase along the eastern Sierra Madre Occidental, and a reduction off the west coast of Mexico. The heating increase over the U.S. Great Plains is associated with the model simulation of the Great Plains LLJ, which is present in the M simulation but not in the noNA simulation, broadly consistent with Ting and Wang (2006). The precipitation changes over and near western Mexico are due to the physical blocking of the moisture-laden trade winds by the Sierra Madre

Occidental; the orographic uplifting of the atmospheric flow facilitates the formation of local precipitation and enhances latent heat release there. Changes in the transient vorticity and heat flux convergences resulting from North American orography are not considered here given that their effects on climatological stationary waves in the summer hemisphere are small overall (Ting et al. 2001; Ting and Wang 2006).

When forced with both North American orography and the orography-induced changes in diabatic heating, the SWM reproduces much of the upper-level stationary wave differences seen between the M and noNA AGCM simulations, particularly the climatological high over North America (cf. Fig. 7d with Fig. 7c). This suggests that the SWM does a credible job of reproducing the orography-related climatological stationary waves in the GEOS AGCM and that any changes in the transient vorticity and heat flux convergences induced by North American orography contribute little to the North American high. Examined together, the B1–B3 SWM experiments show that the North American high is primarily maintained by North American orography interacting with the 3D climatological atmospheric flow from the noNA run (cf. Fig. 7e with Fig. 7d); the modification of diabatic heating resulting from North American orography in fact acts in the opposite direction, forcing an upper-level low over North America (Fig. 7f). Additional SWM experiments forced with regional diabatic heating changes indicate that the low over North America in Fig. 7f is mainly forced by the heating increase over the United States (not shown) and that the contribution from the interaction between the flows forced by North American orography and the orography-induced heating changes is negligible (also not shown). It is worth noting that while the 3D climatological basic state in the noNA simulation has, by construction, no contribution from North American orography, it nevertheless contains substantial zonal variations. The zonal variations over North America and nearby regions are largely forced by the diabatic heating over the Intra-Americas Seas (IAS) and tropical Atlantic regions (not shown), the distribution of which is determined by the land–sea distribution of the North American continent. Therefore, the climatological high over North America is in essence determined by some combination of the local orography and the land–sea distribution of the North American continent, consistent with findings from past studies (e.g., Ting 1994; Ting et al. 2001).

We next examine, through three additional SWM experiments (C1–C3), the relative importance of these two factors in determining the phase locking. The climatological background states used in these three SWM

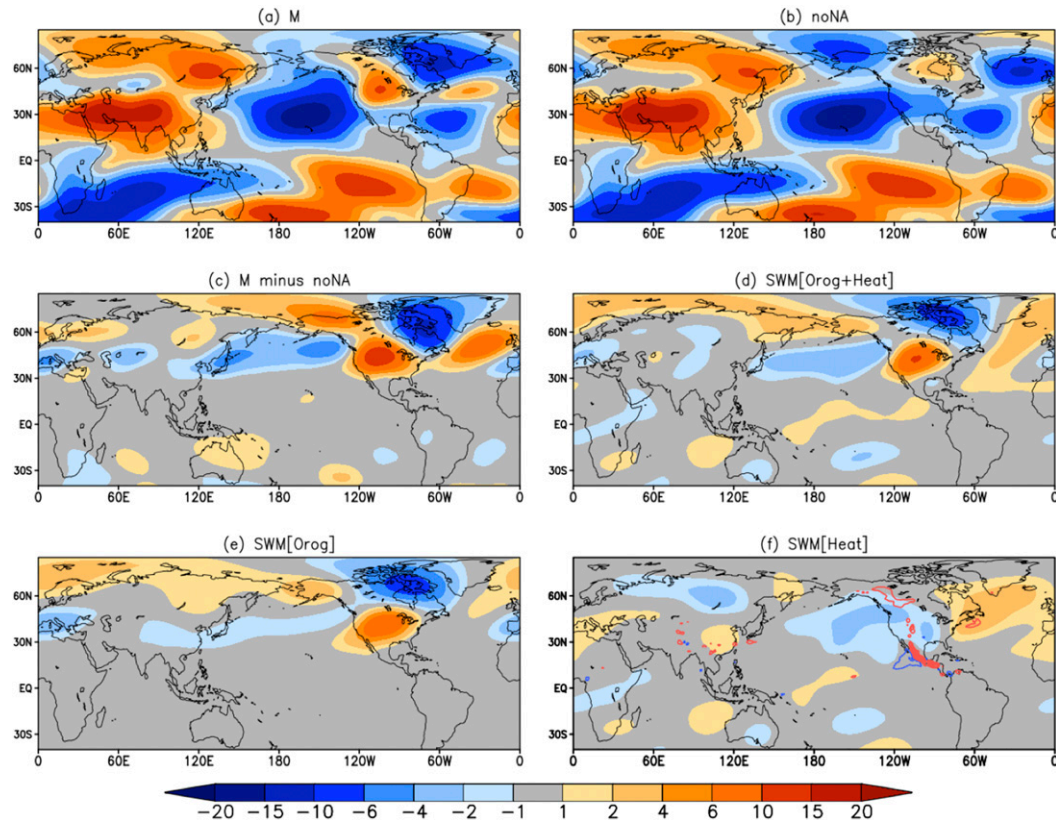


FIG. 7. (a) The JJA climatological (1992–2014) eddy streamfunction ($10^6 \text{ m}^2 \text{ s}^{-1}$) at $\sigma = 0.257$ in the Mountain (M) simulation. (b) As in (a), but for the AGCM simulation that has North American orography removed (noNA). (c) As in (a), but for the eddy streamfunction difference between the M and noNA simulations. (d) The eddy streamfunction response at $\sigma = 0.257$ to the North American orography and the JJA climatological diabatic heating difference between the M and noNA simulations combined, produced by the SWM with a 3D zonally varying climatological JJA basic state from the noNA simulation. (e) As in (d), but for the SWM response to North American orography. (f) As in (d), but for the SWM response to JJA climatological diabatic heating difference between the M and noNA simulations; the JJA climatological heating difference averaged between 600 and 400 hPa is indicated using red contours (contour interval: 1 K).

experiments are respectively (i) the 3D zonally varying climatological basic state from the M simulation, (ii) the 3D zonally varying climatological basic state from the noNA simulation, and (iii) the zonal mean basic state from the noNA simulation. The SWM results with the 3D zonally varying basic state from the M simulation (C1) (Figs. 8a,b) are broadly consistent with those based on MERRA-2 (Figs. 4a,b). The weaker magnitude of the upper-level circulation response from the M simulation (Figs. 8a,b) compared to MERRA-2 (Figs. 4a,b) is presumably due to the GEOS model's underestimation of the summertime jet stream over North America and the North Atlantic. The overall agreement with the MERRA-2 results, however, particularly the reproduction of the upper-level phase-locking signature (Fig. 8b), lends further support for our use of climatological background states

from free-running GEOS AGCM simulations in this investigation.

Figure 8 includes the results of the SWM experiments C2 and C3 as well. The land–sea contrast strengthens the upper-level atmospheric circulation response and reinforces the high anomaly (cf. Figs. 8c,d with Figs. 8e, f); in particular, for the heating anomaly imposed at region 4, it places the high anomaly at the correct geographical location (cf. Fig. 8c with Fig. 8a). Its contribution to the phase locking of the upper-level circulation anomalies, however, is only secondary (cf. Fig. 8b with Fig. 8d); its forced circulation anomalies in general move spatially in tandem with the imposed heating anomalies. A comparison of Figs. 8b,8d, and 8f shows that phase locking is clearly reproduced only when the effects of North American orography are included in the basic state—the orography

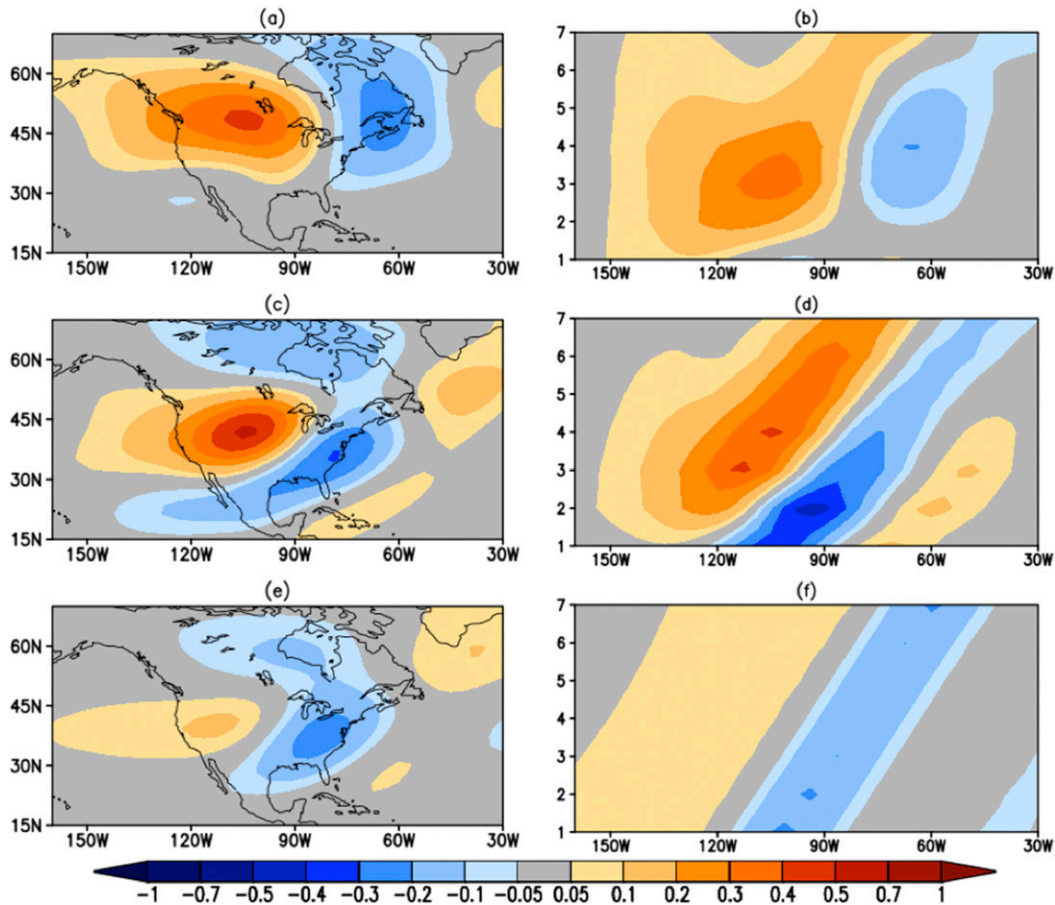


FIG. 8. (a) The eddy streamfunction response at $\sigma = 0.257$ to the idealized diabatic heating anomaly imposed at region 4, produced by the SWM with a 3D zonally varying climatological JJA basic state from the M simulation. (b) The eddy streamfunction response at $\sigma = 0.257$ averaged between 35° and 50°N forced by idealized diabatic heating anomalies imposed at regions 1–7. (c),(d) As in (a) and (b), respectively, but for the 3D zonally varying climatological JJA basic state from the noNA simulation. (e),(f) As in (a) and (b), respectively, but for the zonal mean JJA basic state from the noNA simulation. Unit: $10^6 \text{ m}^2 \text{ s}^{-1}$.

induces phase locking through its maintenance of zonal asymmetries in the basic state, primarily those in air temperature and surface pressure, over North America.

c. Phase locking over other Northern Hemisphere land regions

This subsection extends the investigation to the entire Northern Hemisphere, examining the potential for phase locking in regions outside of North America. The basis of the search for phase-locking behavior is an extensive series of SWM experiments in which regional idealized heating anomalies are imposed (in independent runs) every 7° in latitude and every 7° in longitude across the Northern Hemisphere, using the 3D climatological basic state from MERRA-2 (Table 1). Figure 9 provides a Northern Hemisphere version of

Fig. 4b, the figure with the representative “blocky” pattern that serves as a signature of phase locking (results for latitudes south of 19.5°N show no indication of phase locking and are not included in Fig. 9). The phase-locking signature for North America (centered at 107.5°W on the y axis) is clearly seen in Fig. 9d. Another region with significant phase-locking potential lies in the northern reaches of the Middle East (centered at 42.5°E on the y axis in Figs. 9d and 9e). An imposed heating anomaly over the northern Middle East, regardless of its specific locations, tends to force an upper-level atmospheric circulation anomaly with the same spatial pattern: a high anomaly forms over the northwestern Middle East, with a downstream wave train guided by the summertime South Asian jet (Figs. 10a,b). Figure 9 also offers the hint of a third phase-locking region in Mongolia (centered at 105.5°E on the y axis in Fig. 9e).

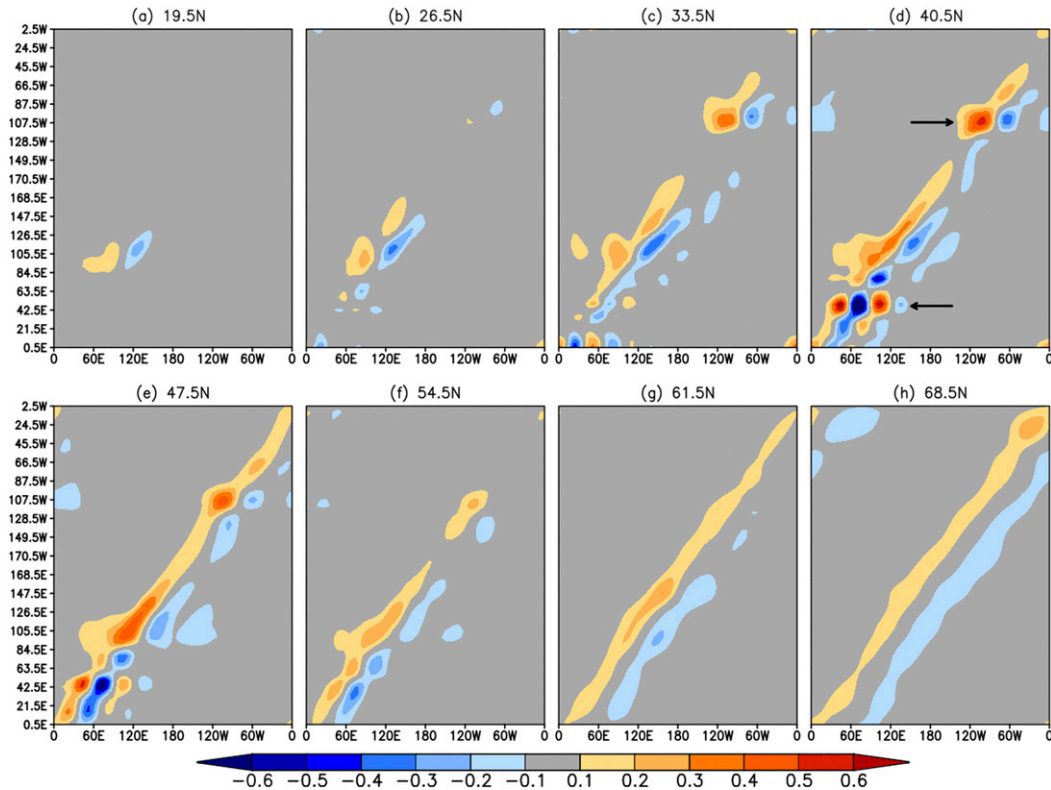


FIG. 9. Identification of regional phase locking over the Northern Hemisphere land using the output of an extensive series of independent SWM runs forced with regional idealized heating anomalies placed every 7° in latitude (0.5° – 357.5° E) and every 7° in longitude (5.5° – 68.5° N) across the Northern Hemisphere; all the SWM runs use a 3D zonally varying climatological JJA basic state from MERRA-2. (a) The eddy streamfunction response at $\sigma = 0.257$ averaged between 20° and 35° N forced by idealized diabatic heating anomalies imposed every 7° in longitude along 19.5° N. The y axis indicates the longitudes that the imposed heating anomalies are centered at; the shading for $y = 42.5^\circ$ E, for example, shows the results for the SWM experiment with the heating anomaly imposed over the $7^\circ \times 7^\circ$ region centered at 19.5° N, 42.5° E. (b) As in (a), but for the SWM responses averaged between 25° and 40° N forced by heating anomalies imposed along 26.5° N. (c) As in (a), but for the SWM responses averaged between 30° and 45° N forced by heating anomalies imposed along 33.5° N. (d) As in (a), but for the SWM responses averaged between 35° and 50° N forced by heating anomalies imposed along 40.5° N. The phase locking over North America and the northern Middle East are marked using black arrows. (e) As in (a), but for the SWM responses averaged between 40° and 55° N forced by heating anomalies imposed along 47.5° N. (f) As in (a), but for the SWM responses averaged between 40° and 55° N forced by heating anomalies imposed along 54.5° N. (g) As in (a), but for the SWM responses averaged between 50° and 65° N forced by heating anomalies imposed along 61.5° N. (h) As in (a), but for the SWM responses averaged between 60° and 75° N forced by heating anomalies imposed along 68.5° N. Unit: $10^6 \text{ m}^2 \text{ s}^{-1}$.

We look now in more detail at the regional phase locking over the northern Middle East, using the methodology we employed above for North America. SWM experiments D2 and D3 were performed with different versions of the climatological basic state; the results, shown in Fig. 10, indicate that local zonal variations of the basic state are critical for the phase locking. Figure 10d shows that the phase locking over the northern Middle East is reproduced when we use the 3D zonally varying basic state over 0° – 65° E and a zonal mean state over 65° E– 360° (D2). However, when we do the reverse—when we use a zonal mean state over

0° – 65° E and the 3D zonally varying state over 65° – 360° E (D3)—the phase-locking signature disappears (Fig. 10f).

A comparison of the M and noIP AGCM simulations (cf. Fig. 7a with Fig. 11a) shows that the Iranian Plateau not only leads to distinct zonal variations of T and P_s (not shown) but also makes a substantial contribution to the upper-level high over the Middle East and extends the climatological stationary waves westward to cover northern Africa (Fig. 11a). The Iranian Plateau also enhances the low-level southwesterlies over the Arabian Sea and northern Indian subcontinent (Fig. 11c) and the accompanying atmospheric moisture transport, contributing to

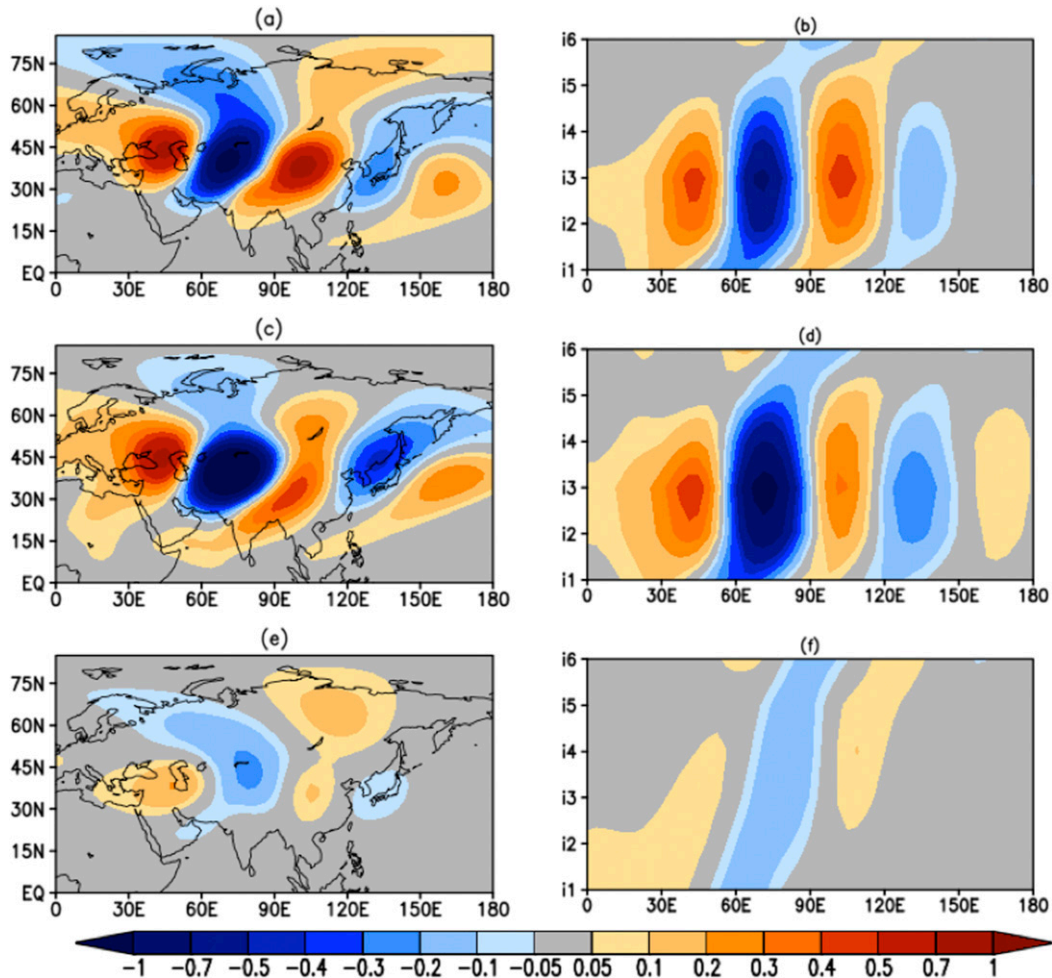


FIG. 10. (a) The eddy streamfunction response at $\sigma = 0.257$ to an idealized diabatic heating anomaly imposed at region i3 produced by the SWM with a 3D zonally varying climatological (1992–2014) JJA basic state from MERRA-2, to illustrate the phase-locked circulation pattern over the northern Middle East. (b) The eddy streamfunction response at $\sigma = 0.257$ averaged between 30° and 60°N for idealized diabatic heating anomalies imposed at regions i1–i6, to demonstrate the phase locking over the northern Middle East. (c), (d) As in (a) and (b), respectively, but using the 3D zonally varying basic state west of 65°E and a zonal mean basic state from MERRA-2 elsewhere. (e), (f) As in (a) and (b), respectively, but using a zonal mean basic state west of 65°E and the 3D zonally varying basic state from MERRA-2 elsewhere. Unit: $10^6 \text{ m}^2 \text{ s}^{-1}$.

the strong latent heat release along the southern edge of the Tibetan Plateau (Figs. 11c). We note that the main features over much of the Northern Hemisphere (Figs. 11b,c) are statistically robust; these JJA features appear even for averaging periods as short as 6 years. These results, based on the GEOS AGCM, are consistent with recent studies using other models (e.g., Simpson et al. 2015; Liu et al. 2017).

The nature of the stationary wave differences between the M and noIP runs (Fig. 11b) is diagnosed by performing three SWM experiments (E1–E3) that use the 3D climatological basic state from the noIP run but are forced with (i) the Iranian Plateau (Fig. 11e),

(ii) the summertime climatological diabatic heating differences between the M and noIP simulations (Fig. 11f), and (iii) these two stationary wave forcings combined (Fig. 11d). When forced with both the Iranian Plateau and its induced diabatic heating changes, the SWM is capable of reproducing much of the climatological stationary wave differences between the M and noIP simulations (cf. Figs. 11b,d). The comparison between Fig. 11d and the SWM responses to the individual stationary wave forcing terms (Figs. 11e,f) shows that the physical barrier imposed by the Iranian Plateau accounts for much of the stationary wave features over the Eurasian continent, which consist of

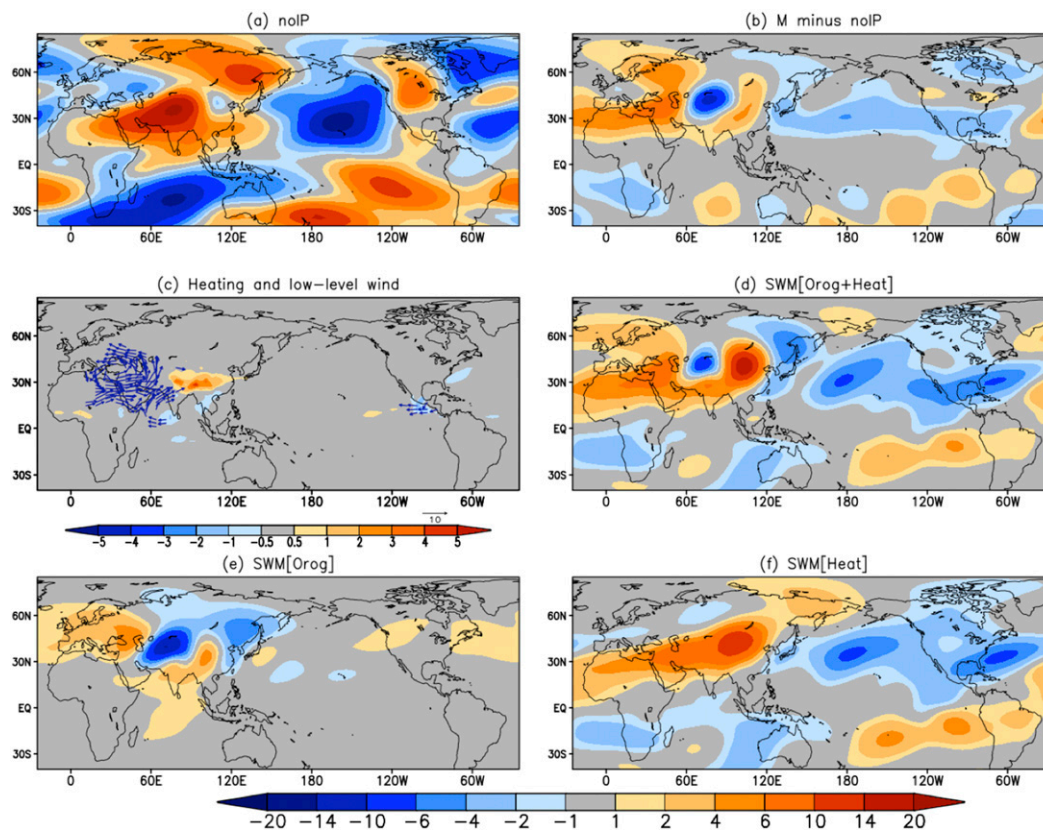


FIG. 11. (a) The JJA climatological (1992–2014) eddy streamfunction ($10^6 \text{ m}^2 \text{ s}^{-1}$) at $\sigma = 0.257$ in the noIP simulation. (b) As in (a), but for the difference between the M and noIP simulations. (c) The JJA climatological difference between the M and noIP simulations in their vertically integrated diabatic heating (shaded; K day^{-1}) and winds at $\sigma = 0.866$ (vector; m s^{-1}); only wind vectors with a magnitude greater than 3 m s^{-1} are shown. (d) The eddy streamfunction response at $\sigma = 0.257$ to the Iranian Plateau and the JJA climatological diabatic heating difference between the M and noIP simulations combined, produced by the SWM with 3D zonally varying climatological JJA basic state from the noIP simulation. (e) As in (d), but for the SWM response to the Iranian Plateau. (f) As in (d), but for the SWM response to the JJA climatological diabatic heating difference between the M and noIP simulations.

an upper-level high over the northern Middle East and a downstream wave train extending across central Asia (Fig. 11e). The diabatic heating, on the other hand, forces a larger-scale upper-level high that stretches across central and southern Asia and extends westward to northern Africa (Fig. 11f). The diabatic heating also accounts for some of the stationary wave features seen across the rest of the globe.

We further investigate the role of local orography, primarily the Iranian Plateau, in inducing the phase locking by performing two additional SWM experiments (F1 and F2), each forced by regional idealized diabatic heating anomalies over the northern Middle East (regions i1–i6 in Fig. 2). The two experiments differ only in the 3D zonally varying climatological basic states used: F1 takes these states from the M (control) simulation, and F2 takes them from the noIP simulation. In these

SWM experiments, phase locking over the Middle East occurs only when the basic state from the M run is used. (A comparison of Figs. 10a and 10b against Figs. 12a and 12b indeed suggests that the free-running GEOS AGCM matches MERRA-2's ability to produce a 3D climatological basic state that leads to phase locking in this region.) When the 3D climatological basic state from the noIP is used, the phase locking over the northern Middle East disappears and the upper-level atmospheric circulation responses themselves are rather weak (Figs. 12c,d). These results suggest that the 3D zonally varying basic state that induces phase locking over the northern Middle East is essentially maintained by the Iranian Plateau. The physical mechanisms operating over the northern Middle East appear to be similar to those over North America; in both cases, regional phase locking is induced by zonal

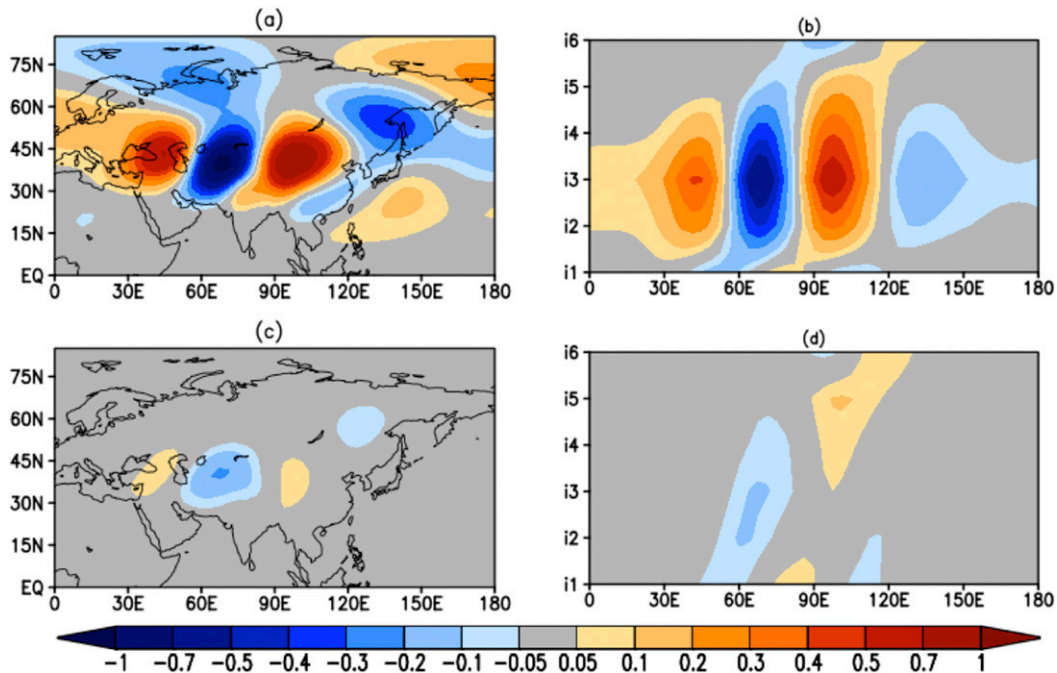


FIG. 12. (a) The eddy streamfunction response at $\sigma = 0.257$ to the idealized diabatic heating anomaly imposed at region i3, produced by the SWM with a 3D zonally varying climatological JJA basic state from the M simulation. (b) The eddy streamfunction response at $\sigma = 0.257$ averaged between 30° and 60°N forced by idealized diabatic heating anomalies imposed at regions i1–i6. (c),(d) As in (a) and (b), but for the 3D zonally varying climatological JJA basic state from the noIP simulation. Unit: $10^6 \text{ m}^2 \text{ s}^{-1}$.

variations in the local basic state that originate from local orography.

4. Summary and discussion

Past modeling analyses have shown that the response of the upper-tropospheric atmospheric circulation to regional dry land surface anomalies in the U.S. continental interior during boreal summer tends to be locked in phase: a high forms over west-central North America and a low forms to the east, regardless of the specific location of the land surface anomaly. This study investigates the causes of this phase locking by isolating those features of the climatological basic state that control it and by determining how these features are maintained. Our results show that the phase locking over North America is induced by zonal asymmetries in the local climatological basic state. Specifically, the zonal asymmetries of T (particularly those in the lower troposphere) and P_s induce the phase locking by placing the soil moisture–forced negative Rossby wave source (dominated by upper-level divergence anomalies) over the eastern leeside of the Western Cordillera, which produces an upper-level high anomaly over west-central North America, with the downstream anomalous

circulation responses phase locked by continuity. The zonal variations of the local climatological atmospheric circulation, manifested as a climatological high over central North America, help shape the spatial pattern of the upper-level circulation responses. It is further found that the relevant zonal asymmetries in the climatological basic state originate from North American orography. The zonal variations of T and P_s directly reflect the impact of orography, while the climatological high over central North America exists as a result of the nonlinear interaction between North American orography and the thermally driven atmospheric flow that impinges on it, supporting previous studies (e.g., Ting 1994; Ting et al. 2001).

While the focus on North America is a natural extension of our efforts to better understand the results of Koster et al. (2016), we also looked more broadly at the phase-locking phenomenon by examining whether other land regions in the Northern Hemisphere exhibit similar behavior, and whether the mechanisms causing the phase locking in these other regions are the same. There is indeed another region in the Northern Hemisphere (the northern Middle East) that exhibits phase locking, and, as in North America, this phase locking is induced by zonal variations in the local basic state resulting from

local orography. It is, however, quite possible that in the northern Middle East, the potential for phase locking will have limited impact on the local atmospheric circulation and hydroclimate. The idealized SWM experiments we performed to address phase locking over the northern Middle East used an imposed heating anomaly appropriate for dry land surfaces over North America (Koster et al. 2016), which may considerably overestimate the actual heating anomalies produced by dry land surfaces in the northern Middle East, which is already climatologically dry. Setting the Middle East question aside, we can at least conclude that, according to our modeling results, orography-induced phase locking does occur over North America—thanks to the Rocky Mountains, North America is one place where soil moisture anomalies have the potential to affect significantly the large-scale circulation.

Acknowledgments. This work has been supported by the NOAA Climate Program Office Modeling, Analysis, Predictions, and Projections (MAPP) program (NA14OAR4310221) and the NASA Modeling, Analysis and Prediction (MAP) program (NNG17HP01C). We thank two anonymous reviewers for their constructive comments and suggestions, which have greatly improved the paper.

REFERENCES

- Bacmeister, J. T., M. J. Suarez, and F. R. Robertson, 2006: Rain reevaporation, boundary layer–convection interactions, and Pacific rainfall patterns in an AGCM. *J. Atmos. Sci.*, **63**, 3383–3403, <https://doi.org/10.1175/JAS3791.1>.
- Bonner, W. D., 1968: Climatology of the low level jet. *Mon. Wea. Rev.*, **96**, 833–850, [https://doi.org/10.1175/1520-0493\(1968\)096<0833:COTLLJ>2.0.CO;2](https://doi.org/10.1175/1520-0493(1968)096<0833:COTLLJ>2.0.CO;2).
- Brayshaw, D. J., B. Hoskins, and M. Blackburn, 2009: The basic ingredients of the North Atlantic storm track. Part I: Land–sea contrast and orography. *J. Atmos. Sci.*, **66**, 2539–2558, <https://doi.org/10.1175/2009JAS3078.1>.
- Broccoli, A. J., and S. Manabe, 1992: The effects of orography on midlatitude Northern Hemisphere dry climates. *J. Climate*, **5**, 1181–1201, [https://doi.org/10.1175/1520-0442\(1992\)005<1181:TEOOM>2.0.CO;2](https://doi.org/10.1175/1520-0442(1992)005<1181:TEOOM>2.0.CO;2).
- Gelaro, R., and Coauthors, 2017: The Modern-Era Retrospective Analysis for Research and Applications, version 2 (MERRA-2). *J. Climate*, **30**, 5419–5454, <https://doi.org/10.1175/JCLI-D-16-0758.1>.
- Helfand, H. M., and S. D. Schubert, 1995: Climatology of the simulated Great Plains low-level jet and its contribution to the continental moisture budget of the United States. *J. Climate*, **8**, 784–806, [https://doi.org/10.1175/1520-0442\(1995\)008<0784:COTSGP>2.0.CO;2](https://doi.org/10.1175/1520-0442(1995)008<0784:COTSGP>2.0.CO;2).
- Kitoh, A., 2002: Effects of large-scale mountains on surface climate—A coupled ocean-atmosphere general circulation model study. *J. Meteor. Soc. Japan*, **80**, 1165–1181, <https://doi.org/10.2151/jmsj.80.1165>.
- Koster, R. D., M. J. Suarez, and M. Heiser, 2000: Variance and predictability of precipitation at seasonal-to-interannual timescales. *J. Hydrometeorol.*, **1**, 26–46, [https://doi.org/10.1175/1525-7541\(2000\)001<0026:VAPOPA>2.0.CO;2](https://doi.org/10.1175/1525-7541(2000)001<0026:VAPOPA>2.0.CO;2).
- , and Coauthors, 2011: The second phase of the Global Land–Atmosphere Coupling Experiment: Soil moisture contributions to subseasonal forecast skill. *J. Hydrometeorol.*, **12**, 805–822, <https://doi.org/10.1175/2011JHM1365.1>.
- , Y. Chang, and S. D. Schubert, 2014: A mechanism for land–atmosphere feedback involving planetary wave structures. *J. Climate*, **27**, 9290–9301, <https://doi.org/10.1175/JCLI-D-14-00315.1>.
- , —, H. Wang, and S. D. Schubert, 2016: Impacts of local soil moisture anomalies on the atmospheric circulation and on remote surface meteorological fields during boreal summer: A comprehensive analysis over North America. *J. Climate*, **29**, 7345–7364, <https://doi.org/10.1175/JCLI-D-16-0192.1>.
- Lin, S.-J., 2004: A vertically Lagrangian finite-volume dynamical core for global models. *Mon. Wea. Rev.*, **132**, 2293–2307, [https://doi.org/10.1175/1520-0493\(2004\)132<2293:AVLFDC>2.0.CO;2](https://doi.org/10.1175/1520-0493(2004)132<2293:AVLFDC>2.0.CO;2).
- Liu, Y. M., Z. Q. Wang, H. F. Zhuo, and G. X. Wu, 2017: Two types of summertime heating over Asian large-scale orography and excitation of potential-vorticity forcing II. Surface heating over Tibetan–Iranian Plateau. *Sci. China Earth Sci.*, **60**, 733–744, <https://doi.org/10.1007/s11430-016-9016-3>.
- Molod, A., L. Takacs, M. Suarez, J. Bacmeister, I.-S. Song, and A. Eichmann, 2012: The GEOS-5 Atmospheric General Circulation Model: Mean climate and development from MERRA to Fortuna. NASA Tech. Rep. Series on Global Modeling and Data Assimilation, Vol. 28, NASA Tech. Memo. NASA/TM–2012-104606, 117 pp.
- Moorthi, S., and M. J. Suarez, 1992: Relaxed Arakawa–Schubert: A parameterization of moist convection for general circulation models. *Mon. Wea. Rev.*, **120**, 978–1002, [https://doi.org/10.1175/1520-0493\(1992\)120<0978:RASAP0>2.0.CO;2](https://doi.org/10.1175/1520-0493(1992)120<0978:RASAP0>2.0.CO;2).
- Nigam, S., I. M. Held, and S. W. Lyons, 1986: Linear simulation of the stationary eddies in a general circulation model. Part I: The no-mountain model. *J. Atmos. Sci.*, **43**, 2944–2961, [https://doi.org/10.1175/1520-0469\(1986\)043<2944:LSOTSE>2.0.CO;2](https://doi.org/10.1175/1520-0469(1986)043<2944:LSOTSE>2.0.CO;2).
- Reynolds, R. W., N. A. Rayner, T. M. Smith, D. C. Stokes, and W. Q. Wang, 2002: An improved in situ and satellite SST analysis for climate. *J. Climate*, **15**, 1609–1625, [https://doi.org/10.1175/1520-0442\(2002\)015<1609:AIIASAS>2.0.CO;2](https://doi.org/10.1175/1520-0442(2002)015<1609:AIIASAS>2.0.CO;2).
- Rienecker, M. M., and Coauthors, 2008: The GEOS-5 data assimilation system—Documentation of versions 5.0.1, 5.1.0, and 5.2.0. NASA Tech. Rep. Series on Global Modeling and Data Assimilation, Vol. 27, NASA Tech. Memo. NASA/TM–2007-104606, 101 pp.
- Rodwell, M. J., and B. J. Hoskins, 2001: Subtropical anticyclones and summer monsoons. *J. Climate*, **14**, 3192–3211, [https://doi.org/10.1175/1520-0442\(2001\)014<3192:SAASM>2.0.CO;2](https://doi.org/10.1175/1520-0442(2001)014<3192:SAASM>2.0.CO;2).
- Sardeshmukh, P. D., and B. J. Hoskins, 1988: The generation of global rotational flow by steady idealized tropical divergence. *J. Atmos. Sci.*, **45**, 1228–1251, [https://doi.org/10.1175/1520-0469\(1988\)045<1228:TGOGRF>2.0.CO;2](https://doi.org/10.1175/1520-0469(1988)045<1228:TGOGRF>2.0.CO;2).
- Schubert, S., H. Wang, and M. Suarez, 2011: Warm season subseasonal variability and climate extremes in the Northern Hemisphere: The role of stationary Rossby waves. *J. Climate*, **24**, 4773–4792, <https://doi.org/10.1175/JCLI-D-10-05035.1>.
- , —, R. Koster, M. Suarez, and P. Groisman, 2014: Northern Eurasian heat waves and droughts. *J. Climate*, **27**, 3169–3207, <https://doi.org/10.1175/JCLI-D-13-00360.1>.
- Simpson, I. R., R. Seager, T. A. Shaw, and M. Ting, 2015: Mediterranean summer climate and the importance of Middle East

- topography. *J. Climate*, **28**, 1977–1996, <https://doi.org/10.1175/JCLI-D-14-00298.1>.
- Ting, M., 1994: Maintenance of northern summer stationary waves in a GCM. *J. Atmos. Sci.*, **51**, 3286–3308, [https://doi.org/10.1175/1520-0469\(1994\)051<3286:MONSSW>2.0.CO;2](https://doi.org/10.1175/1520-0469(1994)051<3286:MONSSW>2.0.CO;2).
- , and L. Yu, 1998: Steady response to tropical heating in wavy linear and nonlinear baroclinic models. *J. Atmos. Sci.*, **55**, 3565–3582, [https://doi.org/10.1175/1520-0469\(1998\)055<3565:SRTTHI>2.0.CO;2](https://doi.org/10.1175/1520-0469(1998)055<3565:SRTTHI>2.0.CO;2).
- , and H. Wang, 2006: The role of North American orography in the maintenance of the Great Plains summer low-level jet. *J. Atmos. Sci.*, **63**, 1056–1068, <https://doi.org/10.1175/JAS3664.1>.
- , —, and L. Yu, 2001: Nonlinear stationary wave maintenance and seasonal cycle in the GFDL R30 GCM. *J. Atmos. Sci.*, **58**, 2331–2354, [https://doi.org/10.1175/1520-0469\(2001\)058<2331:NSWMA>2.0.CO;2](https://doi.org/10.1175/1520-0469(2001)058<2331:NSWMA>2.0.CO;2).
- Tokioka, T., K. Yamazaki, A. Kitoh, and T. Ose, 1988: The equatorial 30–60 day oscillation and the Arakawa-Schubert penetrative cumulus parameterization. *J. Meteor. Soc. Japan*, **66**, 883–901, https://doi.org/10.2151/jmsj1965.66.6_883.
- Yasunari, T., K. Saito, and K. Takata, 2006: Relative roles of large-scale orography and land surface processes in the global hydroclimate. Part I: Impacts on monsoon systems and the tropics. *J. Hydrometeor.*, **7**, 626–641, <https://doi.org/10.1175/JHM515.1>.